

OPTICAL PROPERTIES OF COMPOSITE MATERIALS BASED ON CONJUGATED POLYMERS AS POLY-P-PHENYLENEVINYLENE (PPV) AND ITS DERIVATIVES WITH HIGHLY SEPARATED CARBON NANOTUBES AND GRAPHENES

Mirela ILIE¹

Scientific coordinator: Prof. Univ. Dr. Daniela DRAGOMAN²

October, 2018

1. Introduction

The composite materials based on conjugated polymers became increasingly often used in organic electronic devices due to the polymers' optical, electrical and mechanical properties, and to their advantage in terms of production costs and ease of solution processing.

In this context, this work investigates the influence of carbon nanoparticles, such as single walled carbon nanotubes (SWNTs) and reduced graphene oxide (RGO), on the optical properties of poly (p-phenylenevinylene) (PPV) [1-3].

By increasing the concentration of carbon nanoparticles, important variations were recorded in the relative intensities ratios corresponding to the maxima of PL spectra of composite materials.

This fact can be correlated with a change of the conjugation length of polymers chains due to the presence of these nanoparticles during the conversion process.

The generation of short polymer chains represents an important aspect that must be considered in the luminescence quenching process due to carbon nanoparticles, such as carbon nanotubes and reduced graphene oxide, which are actively involved as acceptors of electrons generated in the PPV polymer due to excitons' dissociation.

The understanding of processes associated with energy transport, in terms of time and distance, is important for the optimization of the composite structure [4].

The investigation of optical processes represents an attractive subject, which deserves to be explored for a better understanding of the luminescence quenching and for the identification of the chemical species involved in this process.

¹National Institute of Materials Physics, 405 A Atomistilor Street, Magurele, Romania.

²University of Bucharest, Faculty of Physics, 405 Atomistilor Street, Magurele, Romania, and Academy of Romanian Scientists, 54 Splaiul Independentei, Bucharest, Romania.

The quenching of luminescence may be based on several processes, such as molecular rearrangement (static process) [5], quenching through contact (dynamic process) [6], electron(s) transfer [7], reactions in the excited phase [8], chemical defects [9] exciton diffusion [10] or Forster energy transfer mechanism [11].

Some of these processes will be investigated through experimental results obtained from PL emission and excitation spectra and from PL measurements recorded under polarized excitation light.

The optical properties of composite materials are directly influenced by the preparation method. Nanocomposites based on conductive polymers can be prepared using different methods, the main ones being colloidal dispersion and in situ polymerisation [12-15].

The majority of dispersion methods lead to non-covalent assembled composites, where the polymer matrix and the filling agent interact through London dispersion forces.

Nevertheless, there is an increased interest regarding the introduction of covalent bonds between the filling agent/carbon nanoparticles and the polymeric matrix in order to promote strong bonds at the interface.

This thesis studies SWNTs as a mixture of carbon nanotubes (33% metallic nanotubes and 66% semiconductor nanotubes) and SWNTs highly separated in metallic nanotubes (M-SWNTs, 98%) and semiconductor nanotubes (S-SWNTs, 99%).

Different composite systems: PPV/S-SWNTs, PPV/RGO, PPV-Py and PPV-Py-RGO (Py is the notation for pyrene), have been investigated from the point of view of synthesis and optical properties.

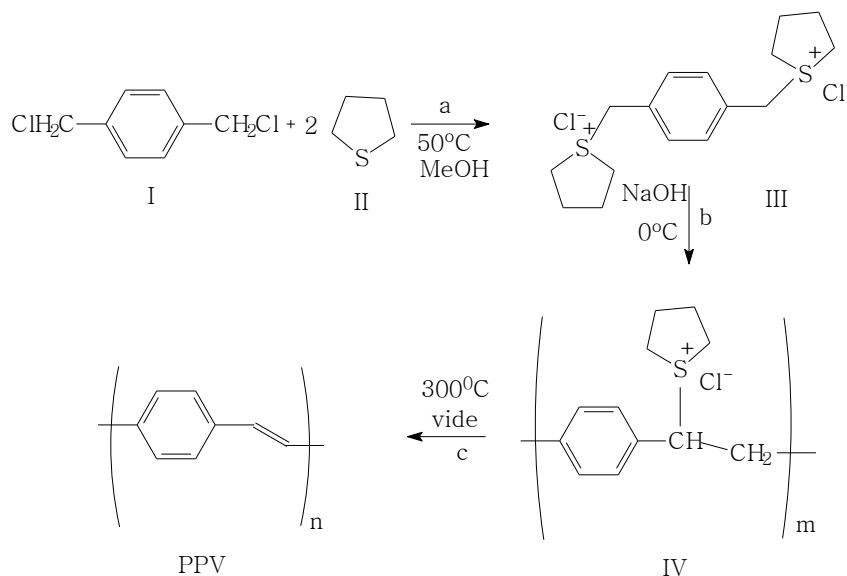
Pyrene has high photoluminescence [16-17], and has proven to be effective for a better homogenization of graphene and carbon nanotubes in solution, thus facilitating the functionalization process of these carbon structures [18].

In addition, the polymers functionalized with pyrene were successfully used for the stabilization of carbon nanotubes in the polymer matrix [18].

Inside the polymer matrix, pyrene plays the role of polarons' stabilizer, allowing a higher ionic mobility than that of the initial macromolecular compound [19-20].

Chapter 1. The synthesis of the poly(p-phenylenevinylene) polymer (PPV)

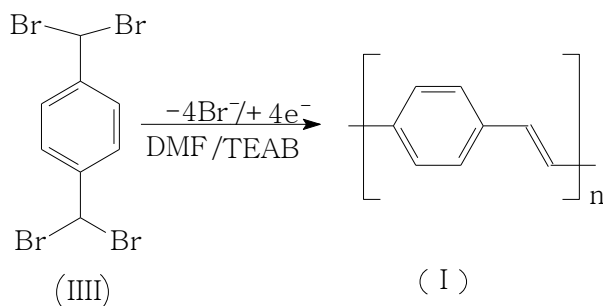
For the synthesis of the PPV polymer, the classic preparation method is the annealing conversion. First step of the synthesis is to prepare the polymer precursor from the α,α' -dichloro-para-xylene and tetrahydrothiophene in methanol, using Wessling-Zimmerman method [15].



Scheme 1. Steps of the PPV precursor synthesis method: (a) the refluxing stage, (b) condensation, (c) annealing conversion of the PPV precursor into the polymer; I, II, III and IV correspond to the following compounds: α,α' -dichloro-p-xylene, tetrahydrothiophene, bisulfonium salt and xylidene sulfonium chloride [21].

In order to convert the PPV precursor into the polymer, the PPV is thermally treated at 300 °C, under vacuum conditions; for preparation of composites, the precursor solution is further mixed with the carbon nanofiller, is ultrasonicated and then thermally treated as specified above. Because of the large amount of chemical reagents used during the PPV's chemical synthesis route and the long period of time needed, an alternative preparation method, i.e., the electrochemical method [22], was proposed.

According to this method, thin films of polymers can be obtained on a Pt electrode through the cathodic reduction of $\alpha,\alpha,\alpha',\alpha'$ -tetrabromo-p-xylene (TBPX) (Scheme 2).



Scheme 2. Electrochemical polymerization of a $\alpha,\alpha,\alpha',\alpha'$ -tetrabromo-p-xylene [22].

PPV is electrochemically obtained from TBPX (0.02 M) and tetrabutylammonium bromide (TBAB) (0.1 M) in dimethylformamide (DMF), in the potential range (-2,+2) V, at a sweep rate of 100 mV/s.

Three electrodes are used in this synthesis method: the gold electrode as working electrode, Ag/AgCl (3M) as a reference electrode, and the counter electrode consisting of a spiral Pt wire.

The reduction process of TBPX comprises two reactions: the first one is represented by the effective reduction of TBPX by accepting two electrons, and thus leading to bromo-quinodimethane, which is further converted to bromopolyxylidene at -0.8 V, and the second one corresponds to the elimination of bromine atoms remained after the first stage and the formation of vinylenic units, at -1.3 V [23].

Through the electrochemical method one can obtain PPV doped with Br⁻ [2] or PPV in the undoped state, depending on the potential value at which the voltammetric cycles (VC) were stopped [24-25].

Chapter 2. The composite materials such as SWNTs functionalized with PPV

Composite materials based on PPV and carbon nanotubes have attracted interest beginning with 1999 [25] due to their high potential for application in solar cell devices.

The composites based on SWNTs and PPV were obtained using the already presented method, i.e. the annealing conversion of the mixture between the PPV precursor and carbon nanotubes followed by the electrochemical reduction of TBPX on the working electrode (Au electrode) modified by depositing a film of (M+S)-SWNTs, M-SWNTs or S-SWNTs on its surface.

According to Figure 1, the presence of TBPX is confirmed by the absorption band situated at 270 nm (4.6 eV). [27]

The UV-Vis absorption spectrum of the electrochemically synthesized PPV deposited on an ITO substrate shows an absorption threshold at 3.23 eV due to π - π^* electronic transitions [28].

The generation of TBPX diradicals is confirmed through an absorption band situated at 3.95 eV (312 nm).

The Raman lines in Figures 2 and 3 corresponding to the radial vibration mode (RBM) of SWNTs situated at 164 and 168 cm⁻¹, are related to carbon nanotubes with diameters of ~1.36 and 1.34 nm, respectively.

The Raman spectra were obtained for an excitation wavelength of 1064 nm.

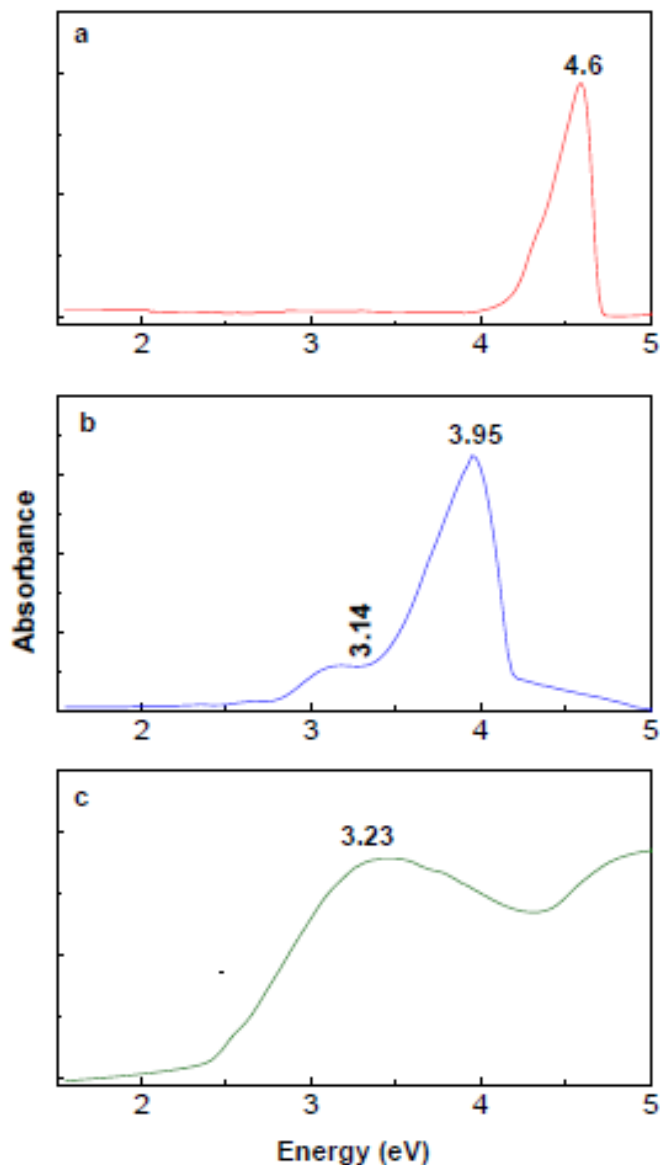


Fig. 1. UV-VIS absorption spectra of the TBPX in the initial state (a) and after the reduction process at -2 V (b). (c) UV-VIS absorption spectrum of PPV deposited on ITO substrate [26]

By increasing the number of VC recorded on gold supports covered with (M+S)-SWNTs and S-SWNTs films, one can observe a gradual decrease in the relative intensity of the RBM line, the appearance of the line situated at 1174 cm^{-1} and the shift to higher wavelength of the defect band (D band) without any variations in intensity. All these variations are consequences of the shielding effect induced by the full coverage of S-SWNTs with PPV macromolecular chains (PPV MC).

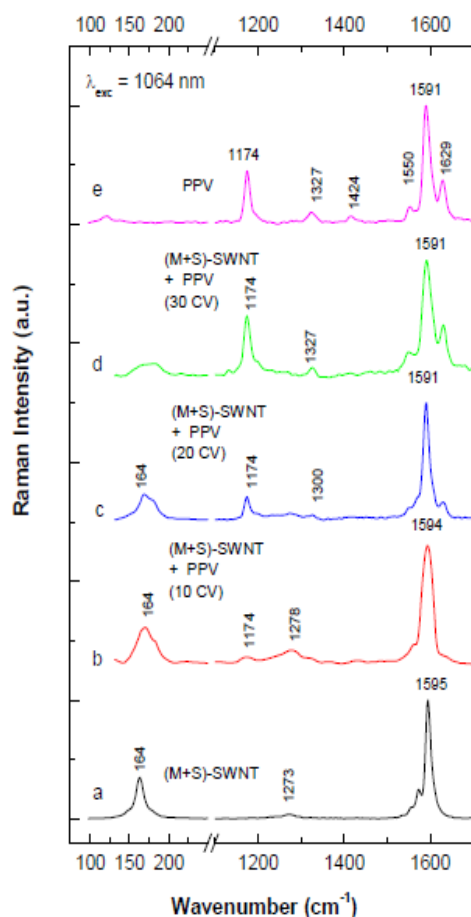


Fig. 2. Raman spectra, at 1064 nm, of (M+S)-SWNTs (a) and its composites with PPV, obtained after 10 (b), 20 (c) and 30 (d) voltammetric cycles (VC); (e) Raman spectrum of PPV [26].

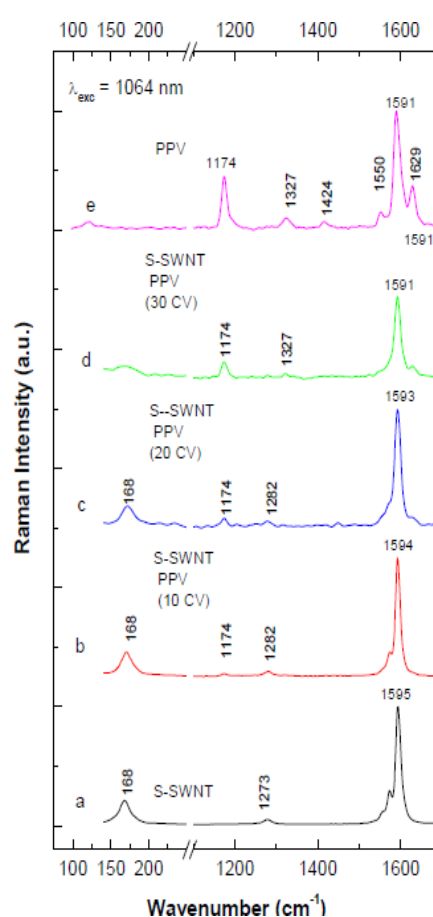


Fig. 2. Raman spectra, at 1064 nm, of S-SWNTs (a) and its composites with PPV, obtained after 10 (b), 20 (c) and 30 (d) voltammetric cycles (VC); (e) Raman spectrum of PPV [26].

Comparing the evolution of (M+S)-SWNTs and M-SWNTs Raman spectra performed at a resonant excitation wavelength for the metallic component, as increasing the concentration of the polymer, one can observe the asymmetric profile of the Raman line situated between 1547-1582 cm⁻¹, which is due to the electron-phonon interaction [29].

The decrease of the intensities of Raman lines situated at 1540 cm⁻¹ and 1547 cm⁻¹, while the RBM intensity remains constant, is associated to the isolation of the individual tubes from the bundles as a result of the functionalization process with PPV (Figures 4 and 5).

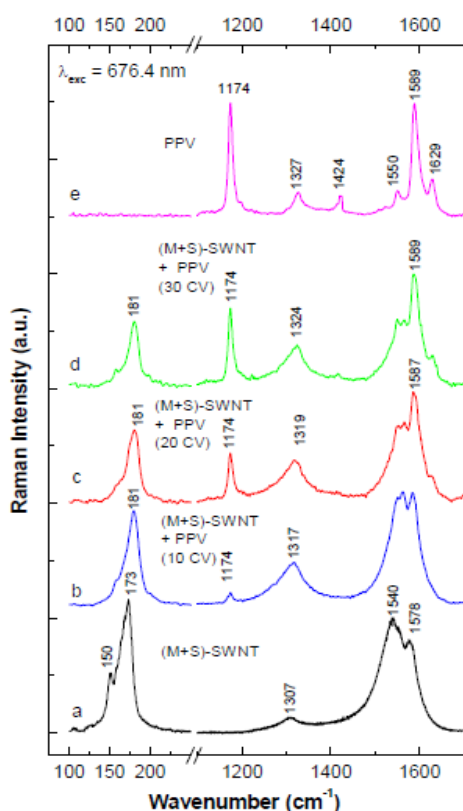


Fig. 3. Raman spectra at an excitation wavelength of 676.4 nm, of PPV (e), (M+S)-SWNTs (a) and its composites after 10 (b), 20 (c) and 30 (d) VC [26].

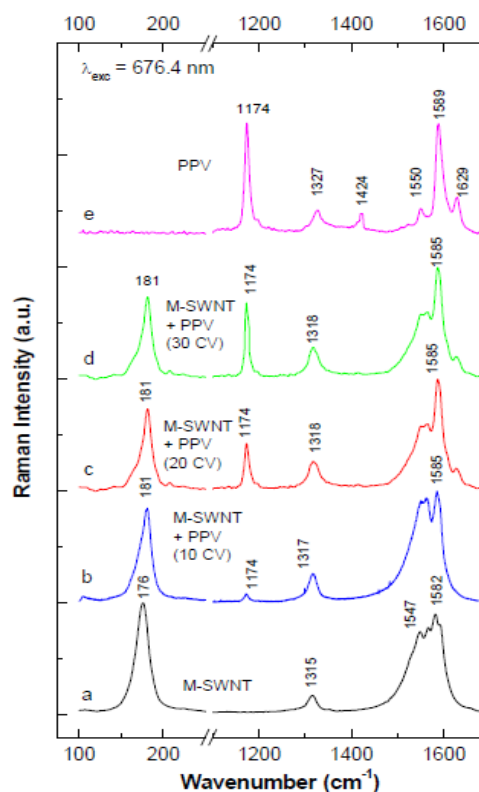


Fig. 5. Raman spectra at an excitation wavelength of 676.4 nm, of PPV (e), M-SWNTs (a) and its composites obtained after 10 (b), 20 (c) and 30 (d) VC [26].

Using the IR spectroscopy one can identify the type of carbon nanotube from the PPV/SWNTs composite: metallic or semiconductor highly separated components (Figure 6). Also, the type of the functionalization process between the SWNTs and PPV depends on the SWNTs predominant component.

Regarding the PPV/M-SWNTs composites, the non-covalent functionalization of M-SWNTs with PPV (Figure 7) is revealed through the presence of two absorption bands located at 1420 and 1452 cm^{-1} , at similar positions as in the case of pristine PPV. On the other hand, the covalent functionalization of S-SWNTs with PPV is revealed through the presence of the IR absorption band, situated at 1471 cm^{-1} , assigned to the deformation vibrational mode of the C-H bond [30]. This type of covalent functionalization takes place through the interaction between the SWNTs cations radicals and the TBPX diradicals during the formation of the polymeric film on the working electrode covered with the S-SWNTs film, when the covalent bond $(\text{C}_{\text{SWNT}})_2\text{-CH}$ is created.

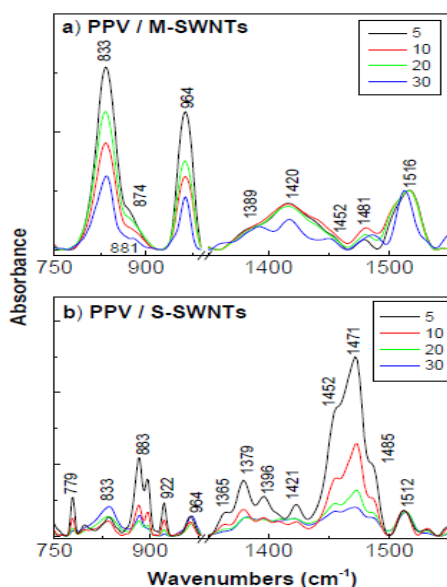


Fig. 4. IR spectra of PPV M-SWNTs (a), electrochemically synthesized on Au electrode covered with S-SWNTs (b) after 5, 10, 20 and 30 VC [27].

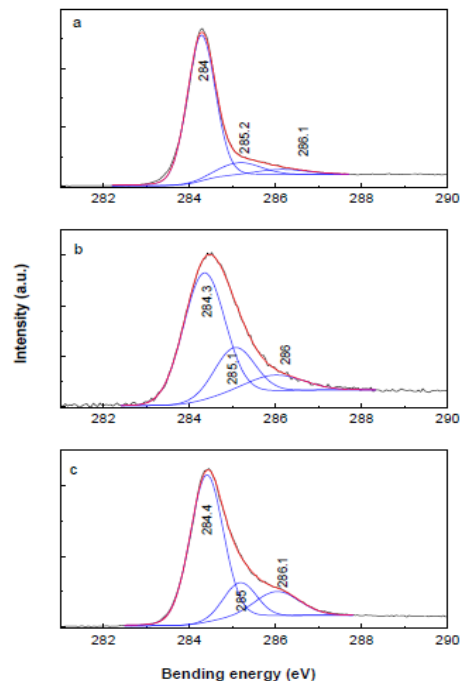


Fig. 7. XPS C_{1s} spectra of S-SWNTs (a), PPV (b) and S-SWNTs covalently functionalized with PPV (c) [27].

Another strong argument, which supports the covalent functionalization of S-SWNTs with PPV, is given by the XPS/C_{1s} spectra recorded on S-SWNTs, PPV and S-SWNTs covalently functionalized with PPV (Figure 7). Comparing the C_{1s} spectrum recorded on S-SWNTs with the one recorded on S-SWNTs covalently functionalized with PPV, one can observe a significant increase in the relative intensity of the band situated at 286.1 eV, which corresponds to the C-C/C-H bond, and a decrease in the relative intensity of the C=C bond situated at 285.2 eV. Those are the most important proofs for the formation of covalent bonds (of C-C and C-Br types) between S-SWNTs and PPV. The distribution of polymer chains of different lengths varies, depending on the type of SWNTs used in the composite (Figure 8).

The luminescence quenching process is visible in all PPV/SWNTs composites, but especially in the case of PPV/M-SWNTs, in which the most pronounced quenching effect was recorded. This fact is explained on the base of the energetic diagram of PPV and SWNTs (33% metallic and 66% semiconducting tubes), S-SWNTs and, respectively, M-SWNTs. According to Figure 9, it can be observed that the LUMO level of PPV is closest to the LUMO level of M-SWNTs compared to all other SWNTs used in the study.

So, the free electrons, originating in the exciton dissociation process, leave the PPV ground state (the HOMO level), then reach the excited state of PPV (the LUMO level) before being promoted to the excited state of M-SWNTs.

After a while the electrons return to the PPV ground state, the energy value of which coincides with M-SWNTs ground state, so that M-SWNTs capture in fact electrons and, as a consequence, the luminescence is quenched.

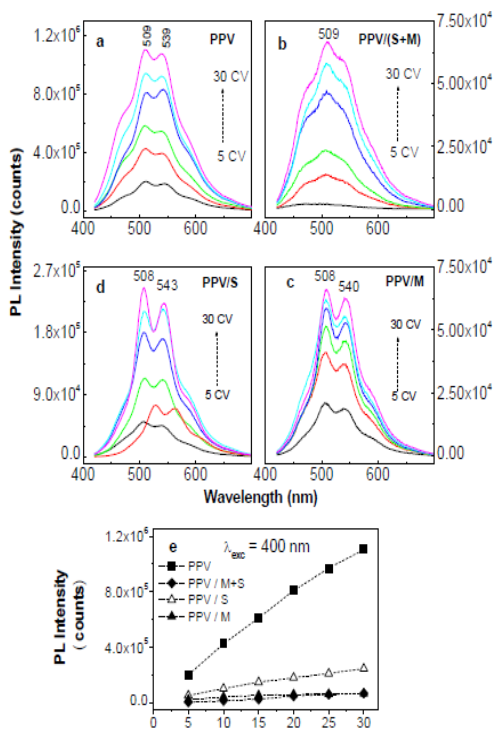


Fig. 8. PL spectra of PPV films electrochemically synthesized on gold electrode before (a) and after the electrode has been covered with (M+S)-SWNTs (b), M-SWNTs (c) and S-SWNTs films (d), after performing 5, 10, 15, 20, 25 and 30 VC; (e) PL quenching of PPV as a function of VC number performed on the gold electrode before and after the electrode has been covered with films of (M+S)-SWNTs, M-SWNTs and respectively S-SWNTS [27].

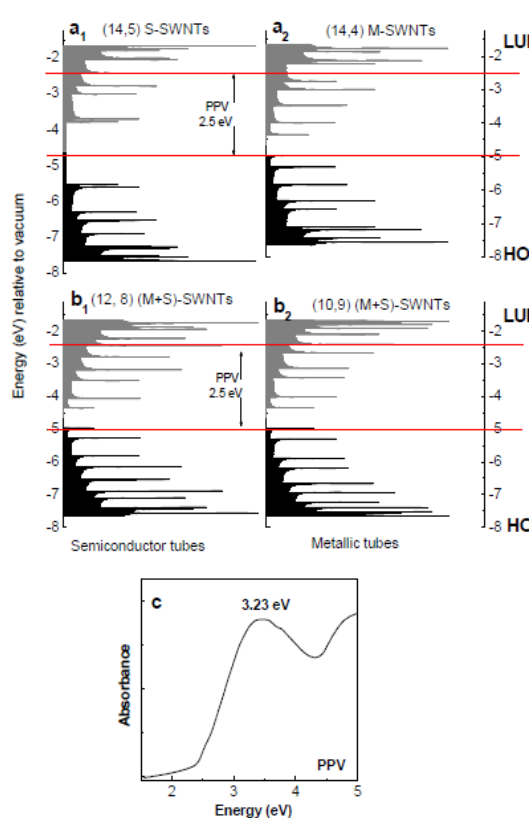


Fig. 9. Diagram of the energy levels of S-SWNTs (a_1), M-SWNTs (a_2) and the metallic (b_2) and semiconductor (b_1) components of (M+S)-SWNTs, as well as of PPV represented by a red line in the figures a_1 , a_2 , b_1 and b_2 . (c) UV-Vis absorption spectra of PPV [27].

Chapter 3. The PPV/RGO composite materials

The PPV/RGO composite materials were also prepared using the same methods as for PPV/SWNTS. In the case of PPV/RGO composites obtained through the annealing treatment, the IR spectra recorded a dependence on the polarization type, s or p, [31-32] and also with the RGO concentration. An increase in the absorbance of the bands situated at 837 and 963-964 cm^{-1} , as the RGO concentration increases, was reported in the PPV/RGO composite prepared through the annealing conversion method similar to SWNTs non-covalently functionalized with undoped PPV [31-33].

The recorded variations of the orientation angle, of 28° and 41°, between the dipolar transition moment vector (θ_{IR}) and the gold supports, for the IR bands situated at ~ 833 -837 and 963-964 cm^{-1} , indicate significant perturbations into the vibrational bending mode outside the plan of the C-H bond of the phenyl ring (Figure 11). Meanwhile, the behavior is totally different in the case of electrochemically synthesized composites. The IR spectra recorded after stopping the VC at +2 V, revealed the IR absorption spectrum of doped PPV. In order to verify the doped character of the obtained PPV, a treatment with NH_4OH was performed. Well known for having an undoping effect, the treatment with NH_4OH reveals the spectrum of undoped PPV, which is different from the spectrum of PPV obtained through annealing conversion. This was the first proof that after the electrochemically synthesis, PPV is not the single product obtained. Many IR bands observed in the PPV spectra after the interaction with NH_4OH are assigned to distyryl benzene (DSB), which has a similar structure, having just three repetitive units of p-phenylenevinylene. Moreover, for the PPV/RGO composite with the highest RGO concentration (0.5 % wt.) a significant increase in the IR absorption band situated at 1417 cm^{-1} , assigned to the bending vibrational mode of the C=C bond from the phenyl ring, was recorded [31-32]. This fact indicates a hindrance effect that appears as a consequence of the covalent functionalization of RGO with undoped PPV.

The type of the functionalization which takes place between the M-SWNTs, S-SWNTs and PPV was also determined through PL anisotropy measurements, also used as a method to determine the wrapping degree of RGO in the PPV polymeric chains.

Therefore, in the case of composite samples prepared through annealing conversion, the reported values of anisotropy (r) are close to 0.4, which indicates that the emission and excitation transition dipoles are aligned and parallel to the basal plane of RGO. On the contrary, in the case of electrochemically synthesized composites, a smaller value of r was reported, which indicates a non-parallel orientation of the emission and excitation transition dipoles.

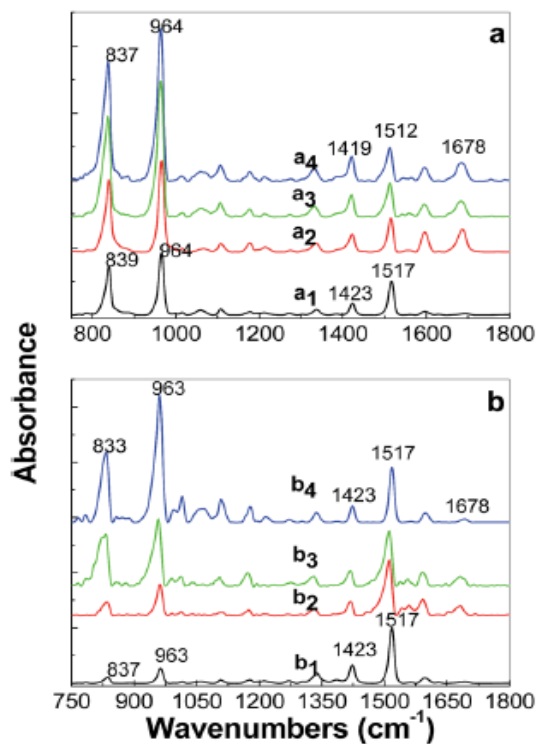


Fig. 5. IR spectra of PPV film obtained through annealing conversion, deposited on gold support, recorded in p (a) and s (b) polarization geometry, in the absence (a_1 and b_1) and in the presence of RGO 0.01 (a_2 , b_2), 0.05 (a_3 , b_3) and 0.1 wt.%(a_4 , b_4) [2].

The values of the wrapping angle of RGO into the PPV chains (θ_{PL}) varied with the RGO concentration, which increased from 0 to 0.5 wt.%, as follows: i) from 12° to 31° , for RGO non-covalently functionalized with undoped PPV; ii) from 28° to 34° , in the case of RGO covalently functionalized with doped PPV.

The increase of θ_{PL} with the RGO concentration is assigned to the appearance of π - π^* interactions between the PPV phenyl group and RGO.

Chapter 4. Composite materials based on PPV, pyrene and RGO

The introduction of pyrene into the PPV matrix leads to inhibition of the polymerization process of the PPV precursor.

This effect was revealed by the appearance of a new line, situated at 613 cm^{-1} (Figure 12) and assigned to the C-S-C vibrational mode of the thiophene ring [34].

The interaction between the phenyl ring of PPV and that of pyrene suggests a non-covalent functionalization process, which takes place through physical π - π interactions.

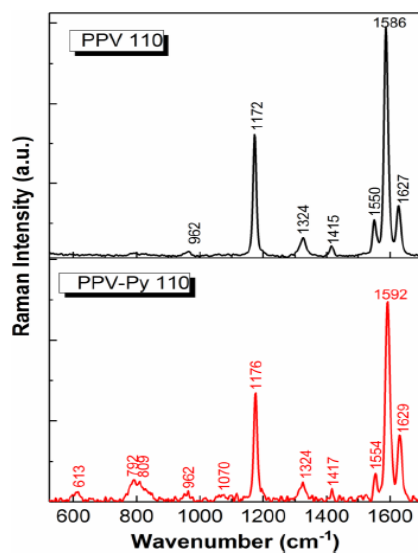


Fig. 12. Raman spectra of PPV and PPV-Py, recorded at 1064 nm excitation wavelength [3].

The interaction between PPV and Py, in the presence of RGO, leads to an increase in the conjugation length, favoring the elimination of the thiophene group.

Chapter 5. Investigation of photoconductive properties of PPV/RGO composite materials

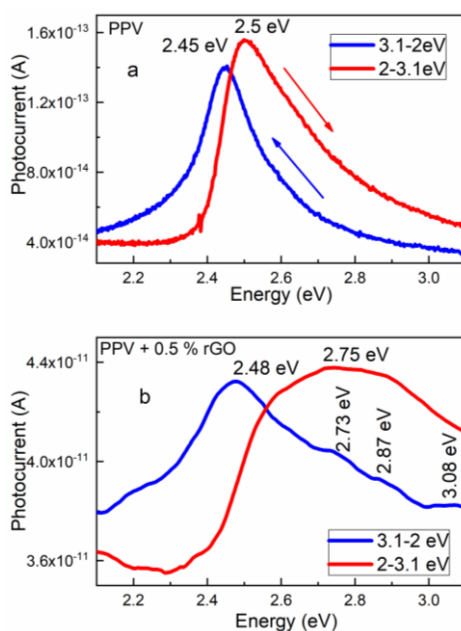


Fig. 13. PC spectra of PPV (a) and its composite with 0.05 wt.% RGO (b) recorded between 2 and 3.1 eV (charge), and reverse (discharge) [36].

By combining the PPV polymer with RGO, one can obtain donor/acceptor materials, where PPV plays the role of donor and RGO the role of electron acceptor [35]. The energetic states of RGO can act as capture centers and also recombination centers for free carriers such as electrons or holes.

Dynamic photocurrent (PC) measurements indicate a lower conduction for pristine PPV, and a PC value with two orders of magnitude higher for PPV/RGO than for PPV. The maxima of the photoconduction spectra, recorded for both sweeping directions of the wavelength, i.e., from 600 to 400 nm and reverse, become larger due to the localized energetic states of RGO (Figure 13).

The generation of the PC is due to the π - π^* transition of free carriers that arrive in the conduction band.

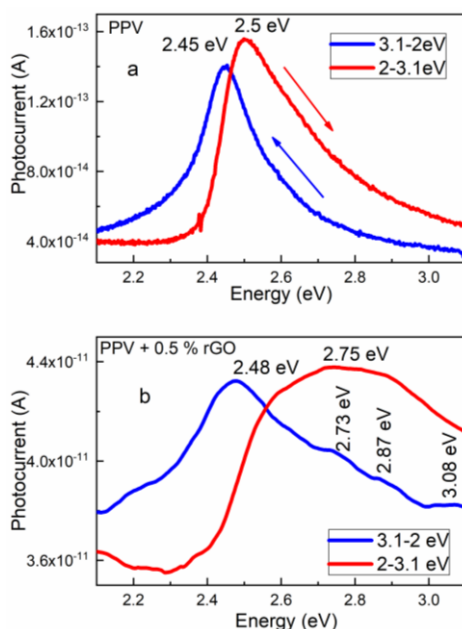
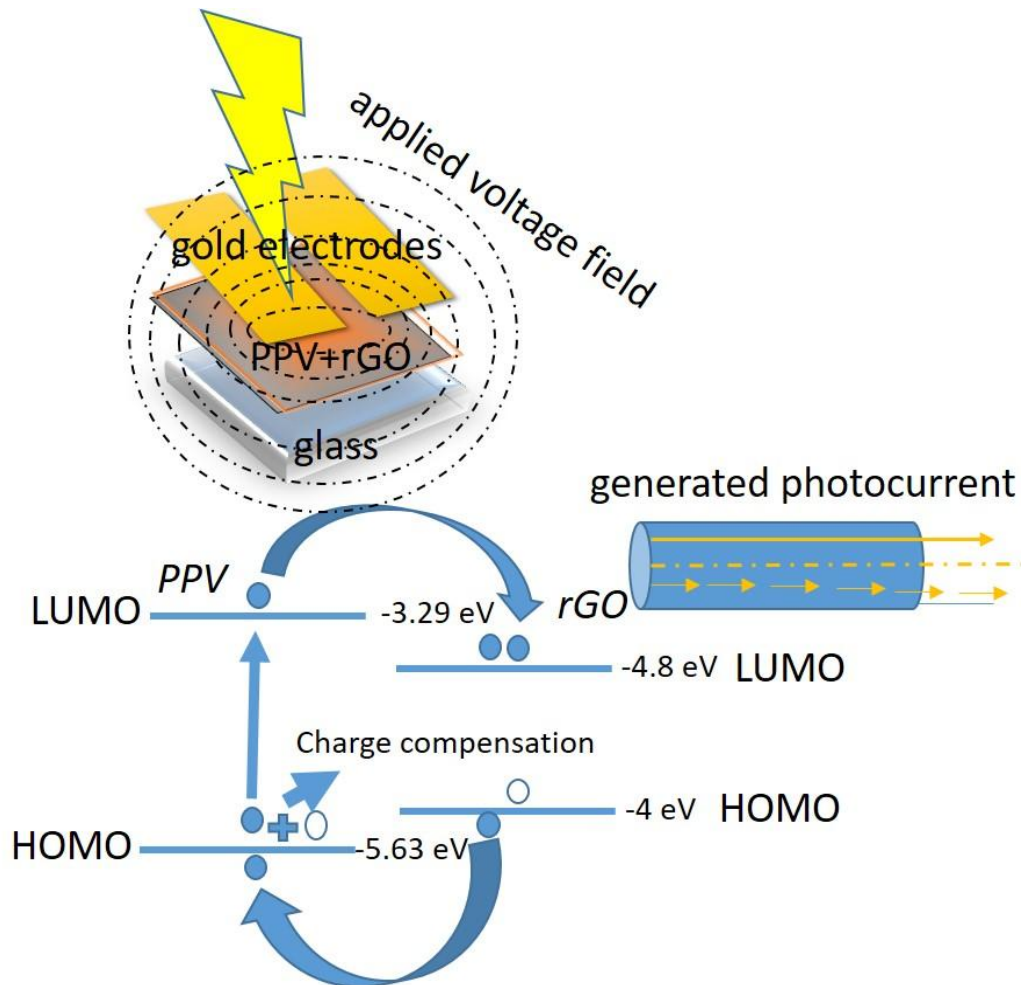


Fig. 13. PC spectra of PPV (a) and its composite with 0.05 wt.% RGO (b) recorded between 2 and 3.1 eV (charge), and reverse (discharge) [36].

The appearance of new maxima in the PPV/RGO PC spectra is mainly visible during the discharge cycle.

These maxima originate in the localized states, which facilitate the charge transfer of the electron from the LUMO level of PPV (equivalent to the conduction band or high energy states) to the LUMO level of RGO. Electrical neutrality is maintained by an electron transfer from the HOMO of RGO (equivalent to the valence band or low energy states) to the HOMO of PPV, where recombination takes place.

The mechanism of charge transfer is illustrated below, in scheme 3.



Scheme 3. The photoconduction mechanism of PPV/RGO composite [36].

To estimate the time spent by the electrons, produced inside the PPV matrix, in the excited state and to identify the type of the RGO localized states, measurements of the photocurrent dynamics were performed.

The purpose of the study is to explain the observed fact that the composite samples remained charged for a while, after cessation of exposure, returning to the initial state after a certain time duration in the absence of light.

In this context the PPV/RGO composites were illuminated with optical pulses and, using the equations:

$$y = y_0 + A_1 e^{-\frac{(x-x_0)}{\tau_1}} + A_2 e^{-\frac{(x-x_0)}{\tau_2}} \quad (1)$$

for the charge process and

$$y = y_0 + (1 - A_1 e^{-\frac{(x-x_0)}{\tau_1}}) + (1 - A_2 e^{-\frac{(x-x_0)}{\tau_2}}) \quad (2)$$

for the discharge process, where y is the PC and y_0 its initial value, the time constants for the charge and discharge processes, τ_1 and τ_2 respectively, were calculated.

These time constants differ from each other through one order of magnitude ($\tau_1 = 10.2$ s and $\tau_2 = 145.8$ s, in the case of PPV with 0.01 % RGO) [36], fact which indicates the existence of two relaxation mechanisms, correlated with the different location of RGO energy states relative to the conduction band of PPV.

The RGO localized states delay the recombination of free carriers at the interface between the composite and the gold electrode, generating photocurrent.

Conclusions

As a result of the investigations presented in this thesis, we have concluded that:

1. The electrochemical reduction of TBPX in the presence of CNTs leads to the appearance of a shielding effect of S-SWNTs due to the full coverage of S-SWNTs with PPV macromolecular chains (PPV MC) and, respectively, an effect of isolation of the metallic carbon nanotubes from the bundle.

2. At the electrochemical synthesis of PPV in the presence of M-SWNTs a non-covalent functionalization process takes place.

As a consequence of the covalent functionalization of S-SWNTs with PPV, a steric hindrance effect appears in the case of PPV/S-SWNTs composites.

3. The luminescence quenching process is visible both in the case of PPV/SWNTs and PPV/RGO composites due to the charge transfer, which takes place from the PPV to SWNTs and, respectively, from the PPV to RGO.

4. The anisotropy values calculated for the PPV and its composites with RGO obtained through annealing conversion are very close to 0.4, which indicates that for a wrapping angle of almost 0°, the emission and excitation dipoles are aligned and parallel with the basal plane of RGO, suggesting that the PPV and its composite are preferentially oriented towards the support.

5. As indicated by Raman and IR spectroscopy, adding pyrene to the PPV matrix leads to a non-covalent process, which occurs through π - π interactions.

6. *The PC value is two orders of magnitude higher for PPV/RGO than for pristine PPV due to delaying of the recombination process at the PPV/electrode interface. This delay is caused by the RGO energy states localized in the vicinity of the PPV conduction band, which capture free electrons, keep them trapped, and release them after a while.*

This mechanism based on two processes of charge and discharge is described by two time constants, τ_1 and τ_2 , on the basis of which it can be said that there are two types of capture centers, situated differently with respect to the PPV conduction band.

REFERENCES

- [1] B.R.H. Mişca, Materiale compozite polimerice, Presa Universitară Clujeană, Cluj, **2001**.
- [2] M. Baibarac, M. Ilie, I. Baltog, S. Lefrant, B. Humbert, RSC Adv., **7**, 6931 (2017).
- [3] M. Ilie, M. Baibarac, Opt. Mater., **72**, 140 (2017).
- [4] W. J. Grzegorzcyk, T. J. Savenije, T.E. Dykstra, J. Piris, J. M. Schins, L. D. Siebbeles, J. Phys. Chem. C, **114**, 5182 (2010).
- [5] E. Rusu, A. Airinei, R. I. Tigoianu, Rom. Biotech. Lett., **16**, Supplement (2011).
- [6] J.R. Lakowicz, Mechanisms and Dynamics of Fluorescence Quenching. In: Principles of Fluorescence Spectroscopy energy transfer, Springer, Boston, MA, **2006**, pp.331-351.
- [7] S. Doose, H. Neuweiler, M. Sauer, Chemphyschem. **10**, 1389 (2009).
- [8] J. R. Lakowicz, Excited-State Reactions. In: Principles of Fluorescence Spectroscopy, Springer, Boston, MA, **1999**, pp. 515-530.
- [9] D.Hiller, J. Lopez-Vidrien, S. Gutsch, M. Zacharias, K. Nomoto, D. Konig, Scientific Reports, **7**, 863 (2017).
- [10] Christopher M. Lawson, Richard C. Powell, Walter K. Zwicker, Phys. Rev. B, **26**, 4836 (1982).
- [11] B. Wallace, P.J. Atzberger, PLoS ONE, **12**, e0177122 (2017).
- [12] A. Ghosh, B. Jana, S. Maiti, R. Bera, H. N. Ghosh, A. Patra, ChemPhysChem, **18**, 1308 (2017).
- [13] F. Shimizu, K. Mizoguchi, S. Masubuchi, K. Kume, Synthetic Met., **69**, 43 (1995).
- [14] J. Roncali, Chem. Rev., **92**, 711 (1992).
- [15] S.Higashika, K. Kimura, Y. Matsuo, Y. Sugie, Carbon, **37**, 354 (1999).
- [16] J. Wery, H. Aarab, S. Lefrant, E. Faulques, E. Mulazzi, R. Perego, Phys. Rev. B, **67**, 115202 (2003).
- [17] E. Gonzalez-Juarez, M. Guizado Rodriguez, V. Barba, M. Melgoza-Ramirez, M. Rodriguez, G. Ramos-Ortiz, J.L. Maldonado, J. Mol. Struct., **1103**, 25 (2016).
- [18] T. Medinger, F. Wilkinson, Transactions of the Faraday Society, **62**, 1785 (1966).
- [19] S. Meuer, L. Braun, R. Zentel, Macromol. Chem. Phys., **210**, 1528 (2009).
- [20] L. Astratinea, E. Magner, J. Cassidy, A. Betts, Electrochim. Acta, **115**, 440 (2014).
- [21] R.A. Wessling, J. Polym. Sci.: Polymer Symposia, **72**, 55, 1985.
- [22] R.A. Wessling, R. G. Zimmerman, 3706677 US, 1972.
- [23] H. Nishihara, T. Masahiro, A. Kunitsugu, O. Toshiyuki, K. Okitoshi, Chem. Lett., **16**, 539 (1987).
- [24] J.H.P. Utley, Y. Gao, J. Gruber, Y. Zhang, A. Munoz-Escalona, J. Mater. Chem., **5**, 1837 (1995).

-
- [25] L.O. Peres, H. Varela, J.R. Garcia, M.R. Fernandes, R. M. Torresi, F.C. Nart, J. Gruber, *Synthetic Met.*, **118**, 65 (2001).
- [26] H. Ago, M.S.P. Shaffer, D.S. Ginger, A.H. Windle, R.H. Friend, *Phys. Rev. B*, **61**, 2286 (2000).
- [27] M. Baibarac, I. Baltog, M. Ilie, B. Humbert, S. Lefrant, C. Negrila, *J. Phys. Chem. C*, **120**, 5694 (2016).
- [28] M.A. Miranda, J. Perez-Prieto, E. Font-Sanchis, J. C. Scaiano, *Chem. Commun.*, 1541 (1998).
- [29] E. Mulazzi, A. Ripamonti, J. Wery, B. Dulieu, S. Lefrant, *Phys. Rev. B*, **60**, 16519 (1999).
- [30] Z. Wu, S. Wu, Y. Liang, *Spectrochim. Acta A*, **59**, 1631 (2003).
- [31] D.D.C. Bradley, R.H. Friend, H. Lindemberger, S. Roth, *Polymer*, **27**, 1709 (1986).
- [32] L. Orion, J. P. Buisson, S. Lefrant, *Phys. Rev. B*, **57**, 7050 (1998).
- [33] M. Baibarac, I. Baltog, J. Wery, S. Lefrant, J.Y. Mevellec, *J. Phys. Chem. C*, **116**, 25537 (2012).
- [34] R.P. Hirschmann. "The vibrational spectra of alkyl isocyanates, isothiocyanates and thiocyanates "Retrospective Theses and Dissertations,. Ph. D. Thesis. Michigan : Iowa State University of Science and Technology, **1963**.
- [35] Z. Gan, J. Guo, Y. Di, R. Li, S. Huang, *Phys. Status Solidi B*, **253**, 1138 (2016).
- [36] M. Ilie, D. Dragoman, M. Baibarac, *Phys. Status Solidi B*, 1800392 (2019).